So Messenger readers beware: here is your best chance ever to make your image known to future generations! I am told that portraits can be sent as gifts or on loan only; in the latter case, they will be returned within a month after having been copied. Subject to any restrictions imposed by the donors, the Archenhold Observatory is prepared to supply on request copies of portraits held by them and will issue lists of their holdings from time to time. That is a most useful offer for all who have to write an article or give a talk about the past of their observatory, etc.

The address is: Prof. Dr. D.B. Herrmann, Archenhold-Sternwarte, Alt-Treptow 1, DDR-1193 Berlin, German Democratic Republic. They will be happy to hear from you.   *The editor*

Jacques Beckers Elected to Dutch and Norwegian Academies

On August 28, Queen Beatrix of the Netherlands confirmed the election of ESO staff member Jacques Beckers as "Correspondent" of the Division for Sciences of the Royal Academy of Sciences of the Netherlands. Corresponding members are researchers with a degree from a university in the Netherlands, residing abroad.

Jacques Beckers, who joined ESO in 1988 to become Head of the Interferometry Group, also became a foreign member of the Mathematics-Physics Sciences Division of the Norwegian Academy of Sciences last year.

Our best congratulations to Jacques at the time of these well-deserved honours!
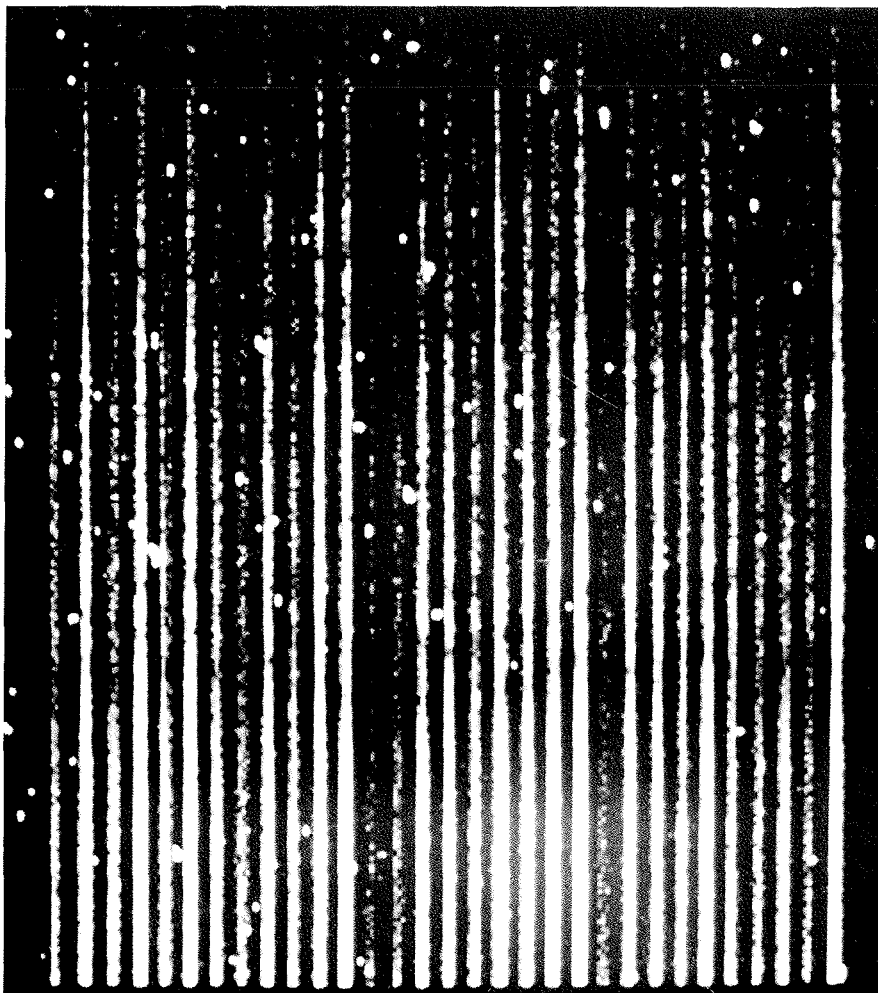
The Efficiency of OPTOPUS

This is part of an OPTOPUS frame resulting from an exposure of galaxies in the cluster Abell 3158, as obtained during the first run (in September 1989) of the ESO Key Programme on "Structure and Dynamics of Rich Clusters of Galaxies".

Note that only the blue parts of the 31 spectra (of 28 galaxies and 3 "skies") are shown in this picture, which covers the wavelength range from ~383 nm (top) to ~440 nm (bottom). The bluest CaII doublet (about one third of the way down) is from sky; the redder CaII doublet (about two thirds of the way down) is from the galaxies, and visually displays the dispersion of the radial velocities of the galaxies in the cluster.

In total, 37 exposures were obtained during the run, which yielded a total of about 1000 galaxy spectra.   *P. Katgert (Leiden)*

An Accurate Wavelength Calibration of CCD CASPEC Echelle Spectra

H. HENSBERGE[1], W. VERSCHUEREN[2]

[1]*Koninklijke Sterrenwacht van België, Brussels, Belgium*
[2]*Theoretical Mechanics and Astrophysics, University of Antwerp (RUCA), Belgium*

Introduction

In December 1986 and January 1988 we obtained with CASPEC at the 3.6-m telescope spectra of early-type member stars of the young stellar cluster NGC 2244 with the main purpose of determining accurate radial velocities. We focused our attention on the blue wavelength region (3700–4700 Å) and used CCD # 3 in combination with the 52 l/mm echelle grating.

For the study of the internal kinema-

tics of the cluster and dealing with relatively few lines in early-type stars, it is evidently of primary interest to achieve high precision in the wavelength calibration, particularly avoiding systematic errors with wavelength. Th-Ar calibra-

tion spectra were obtained before and after every stellar exposure, in the corresponding telescope position. The internal consistency obtained from comparing measured line positions on subsequent calibration frames, after allowance was made for a small shift of the spectrum over the CCD (of the order of a few 10^{-2} pixel in the wavelength direction), is roughly 0.03 pixel in agreement with Monte Carlo simulations taking into account photon noise and read-out noise.

However, in a first reduction using standard MIDAS procedures we noticed that the r.m.s. of the residuals between fitted and theoretical wavelengths was much larger, of the order of 0.15 pixel (0.02 Å) in accordance with the results mentioned by D'Odorico and Ponz (1984). These residuals are obviously not representing random errors, but systematic trends as one might check by comparing the residuals for a given line on various frames. This contribution points out the origin of these systematic errors and describes our solution to the problem.

Analysis of Standard MIDAS Wavelength Calibration Procedure

The standard MIDAS procedure defines the actual position of the Th-Ar lines in the extracted orders by default as the centre of gravity of the two brightest pixels relative to the third brightest. (The more experienced user can use gaussian fitting by specifying his choice in the MIDAS procedure ECHSEAR.) It then identifies the lines, after elimination of resolved doublets, and in the case of theoretical close doublets with components of comparable strength, it couples the line position to a weighted mean wavelength. Finally, it predicts $\lambda_m(x)$ as a function of position x in order m *for each order independently* by fitting a third degree polynomial in x. If less than 4 lines are identified in a given order, a lower degree polynomial is chosen or, when less than 2 lines are identified, ultimately a global first approximation fit with 6 coefficients is used.

Two kinds of systematic errors are introduced by using the standard calibration method, one associated with the actual definition of line centre, the other with the inadequate treatment of line blending. Depending on the desired wavelength accuracy, one might consider these errors either negligible or inadmissible.

In order to illustrate the kind of systematic error introduced by the "gravity" method used to determine line centre, we calculated the theoretical difference between the exact and the "gravity" pre-

dicted line centre position for gaussian lines as a function of the position of the exact line centre relative to the centre of the pixel on which the line was found. Figure 1 shows that the usefulness of the "gravity" method strongly depends on FWHM, producing systematic errors of order 10^{-2} pixel for FWHM = 1 pixel

but of order 10^{-1} pixel for FWHM = 2 pixels. The global effect of "gravity" is that the line is seen closer towards the pixel edge than is actually the case (FWHM > 0.9), an effect that might be empirically illustrated by forming a histogram of the "gravity" measured line centre-to-pixel centre positions (Fig. 2).

Figure 1: *Systematic errors induced by the "gravity" method depending on true line centre-to-pixel centre position. Curves labelled with FWHM refer to theoretical calculations for gaussian lines. Dots resp. circles refer to empirical relations deduced from blue 52 l/mm resp. red 31 l/mm echelle CASPEC data on CCD # 3.*
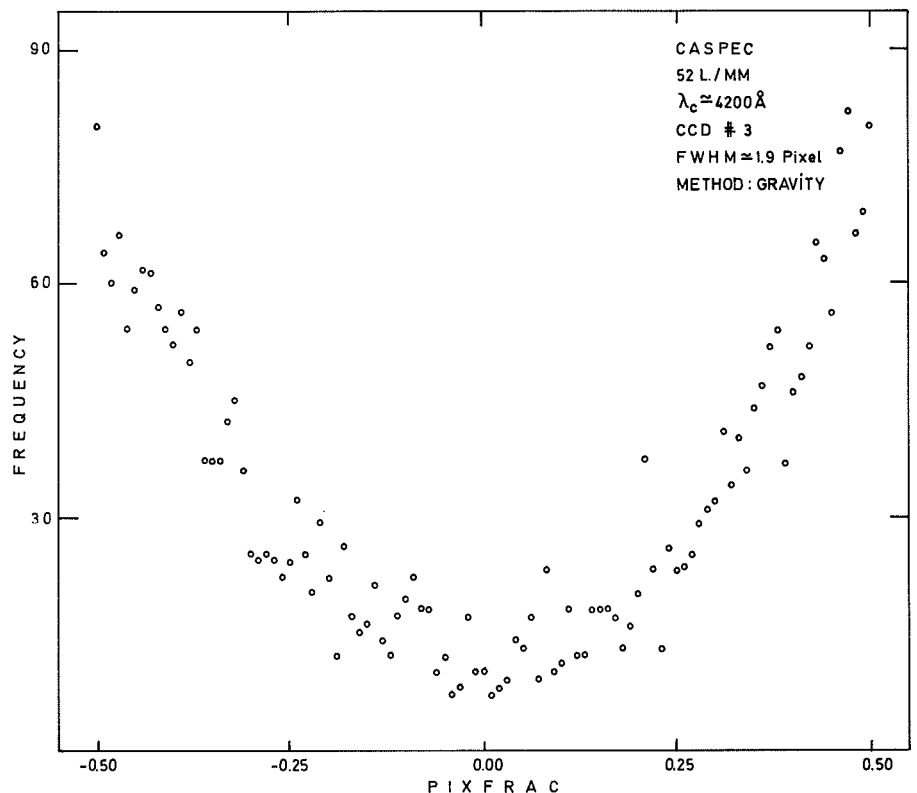
Figure 2: *Distribution of "gravity" measured line positions relative to pixel centre (0.0), summed over 18 calibration frames.*
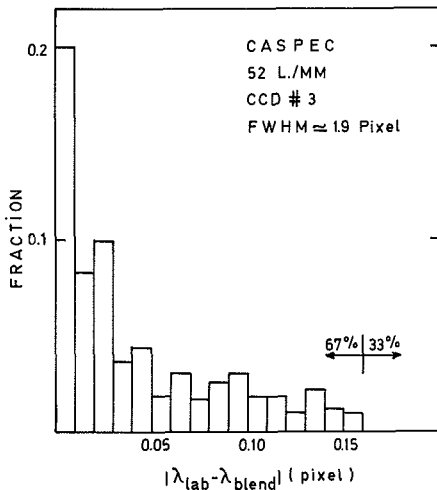
Figure 3: *Distribution of the offsets caused by line blending in the thorium spectrum between 3700 and 4700 Å for gaussian fitting over 5 pixels at the indicated instrumental configuration. Only lines strong enough to be detectable with CASPEC were retained as primary component.*

The thorium spectrum is rich in spectral lines, especially in the blue. When aiming at position accuracies of a few 10^{-3} Å, even weak blends should be taken into account. Convolution of the laboratory thorium spectrum (Palmer and Engleman, 1983) with a point-spread function (PSF) representative for our data and subsequent gaussian line fitting shows that two third of the measured line positions for lines detectable in the CASPEC calibration spectra differ by more than 0.025 pixel (0.003 Å) from their theoretical position (Fig. 3). One third of all lines give offsets larger than 0.15 pixel (0.02 Å). Only a very small fraction of these blends is avoided in the current procedure. Effects of the order of 0.1 pixel are commonly caused by spectral lines one order of intensity fainter than the line they disturb.

It is obvious that line blending and "gravity" line fitting cause errors of the order of the r.m.s. measured using the standard MIDAS wavelength calibration procedure. Thus this r.m.s. does not reflect information on the ultimately obtainable accuracy. More seriously, these approximations have impact on the final wavelength calibration, on the order of a few km s^{-1}. We will not develop here the statistical arguments in support of this statement, but we will illustrate it at the end of the next section (Fig. 6) when discussing one of our calibration frames.

An Improved Wavelength Calibration Procedure

There is no essential argument against the definition of the actual line position of the Th-Ar lines by gaussian (or PSF) fitting. The possibility of gaussian fitting is available in MIDAS, except for the fact that the standard gauss fitting routines in the current echelle package are not intended to deal with undersampled gaussians, nor to treat all kinds of input data substantially differing from pure gaussians. We removed these limitations by an extension of the convergence criteria, an improvement of the initial guesses for the fit parameters and the introduction of the finite pixel size in the computation of the gaussian fit function and its derivative.

The line blending problem calls for a scrutiny of the available calibration tables (LINCAT tables in the MIDAS environment). With the majority of the lines more or less seriously affected by blends, the choice is somewhere in between adopting corrections to the laboratory wavelengths according to the instrument's characteristics and the applied reduction procedure, or selecting a relatively small number of almost unblended lines. The weak points of the first choice are the dependence of the corrections on line strengths (which may vary with age, temperature, internal pressure, etc. of the lamp) as well as on measurement and reduction parameters (PSF, line centre-to-pixel centre position, window used in fitting). The selection possibility on the other hand reduces the number of available calibration lines substantially and creates the need for a global wavelength calibration in order to prevent errors from fitting small numbers of lines in each order to become the major error source (in our set-up the frame includes 21 orders i.e.

84 coefficients to be determined in the standard MIDAS procedure).

We performed theoretical and empirical tests, fully independent from r.m.s. considerations, to build a system for calibration line selection that allows as much freedom as possible to the potential user. On the one hand, we degraded the laboratorium thorium spectra according to our instrumental set-up and calculated blend-induced offsets $\delta\lambda$ for several line centre-to-pixel centre positions by gaussian fitting using windows including up to 7 pixels. On the other hand, we searched empirically for evidence of blends by exploiting the different sensitivity for asymmetries of the "gaussian" and the "gravity" methods. The latter test has been performed on 3 complementary frames i.e. each shifted by $\frac{1}{3}$ pixel in order to achieve optimal results (the detection sensitivity for a particular blend depends strongly on line centre-to-pixel centre position). The test is inherently insensitive to close blends (separation much less than one pixel) and is noise-limited. If one wants to be reasonably confident that the final r.m.s. is not dominated by uncertainties in the corrected laboratory wavelengths, the range of allowed corrections $\delta\lambda$ should be not much larger than the expected r.m.s. and its associated uncertainty ε certainly not larger than half that value. In our case, we selected about 85 lines using $|\delta\lambda| < 5\ 10^{-3}$ Å, $0 \leq \varepsilon \leq 1.5\ 10^{-3}$ Å to have a reasonable frame coverage (Fig. 4) and checked a posteriori that relaxing the criteria up to $|\delta\lambda| < 2\ 10^{-2}$ Å and $0 \leq \varepsilon \leq 2\ 10^{-3}$ Å did not change the wavelength calibration solu-
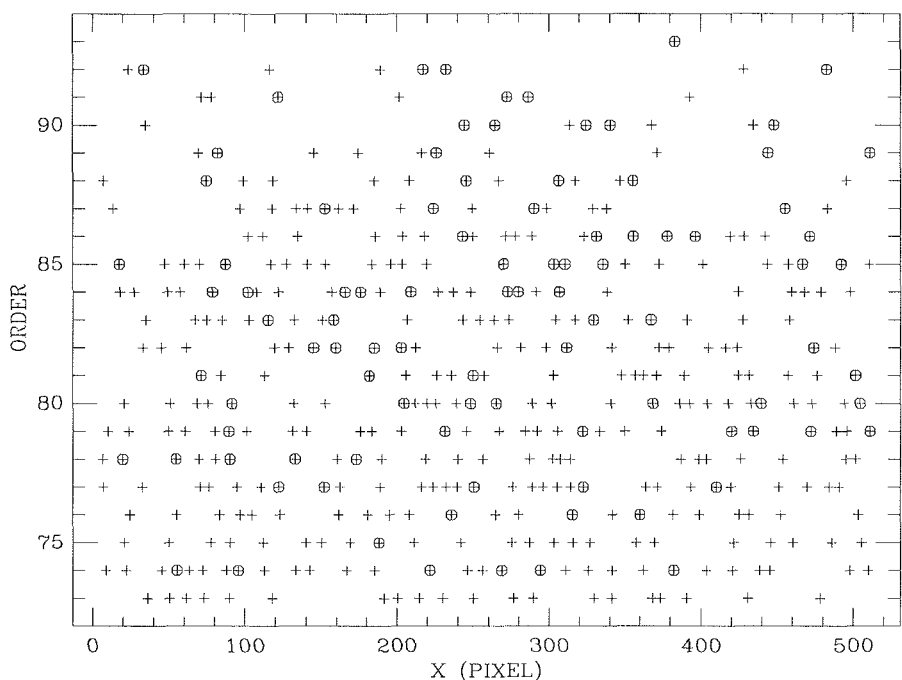
Figure 4: *Distribution of identified (+) and selected lines (encircled).*

tion discussed hereafter although the inclusion of about 25 additional lines did enhance slightly the r.m.s. of the fit. The calibration solution itself remained stable with respect to the line selection as long as it was stringent enough to exclude lines whose assumed (blend)-wavelength is presumably wrong by at least 4 to 5 times the noise-expected uncertainty. The information content of the computed r.m.s. however does depend more critically on the selection and the r.m.s. rises strongly when the conditions on ε are further relaxed.

The calibration has been made finally using a *global fit* of the form

$$\lambda\,(x,\,m^*) = \frac{a_0 + (a_1 + b_1 m^*)\,x + a_2 x^2 + a_3 x^3}{1 + c_1 m^*}$$

with m^* = constant-m, conform to the MIDAS order renumbering, equal to 1 for the highest observed order (the constant being 94 in our case) and x running from 1 to 520 (CCD # 3) defining the actual position of the line centre along the extracted order m^*. Table 1 lists approximate values for the coefficients obtained for two frames taken in different runs. Notice that the term in m^* in the nominator reduces the r.m.s. of frame 2 very significantly, while it is more or less insignificant in the fit of frame 1.

Figure 5 compares the residuals relative to this global fit with selected lines against the residuals obtained using the standard MIDAS procedure, however with the "gravity" method already replaced by gaussian fitting. It illustrates the dominant contribution of line blending to the r.m.s. Moreover, notice in Figure 5a the correlation between low residuals and small numbers of lines for $m \geq 88$, characteristic for overfitting of the data.

Figure 6 shows the wavelength differences generated by these fits at corresponding positions in the frame. Differences of 1 to 2 km s^{-1} are very common, while the r.m.s. of almost un-
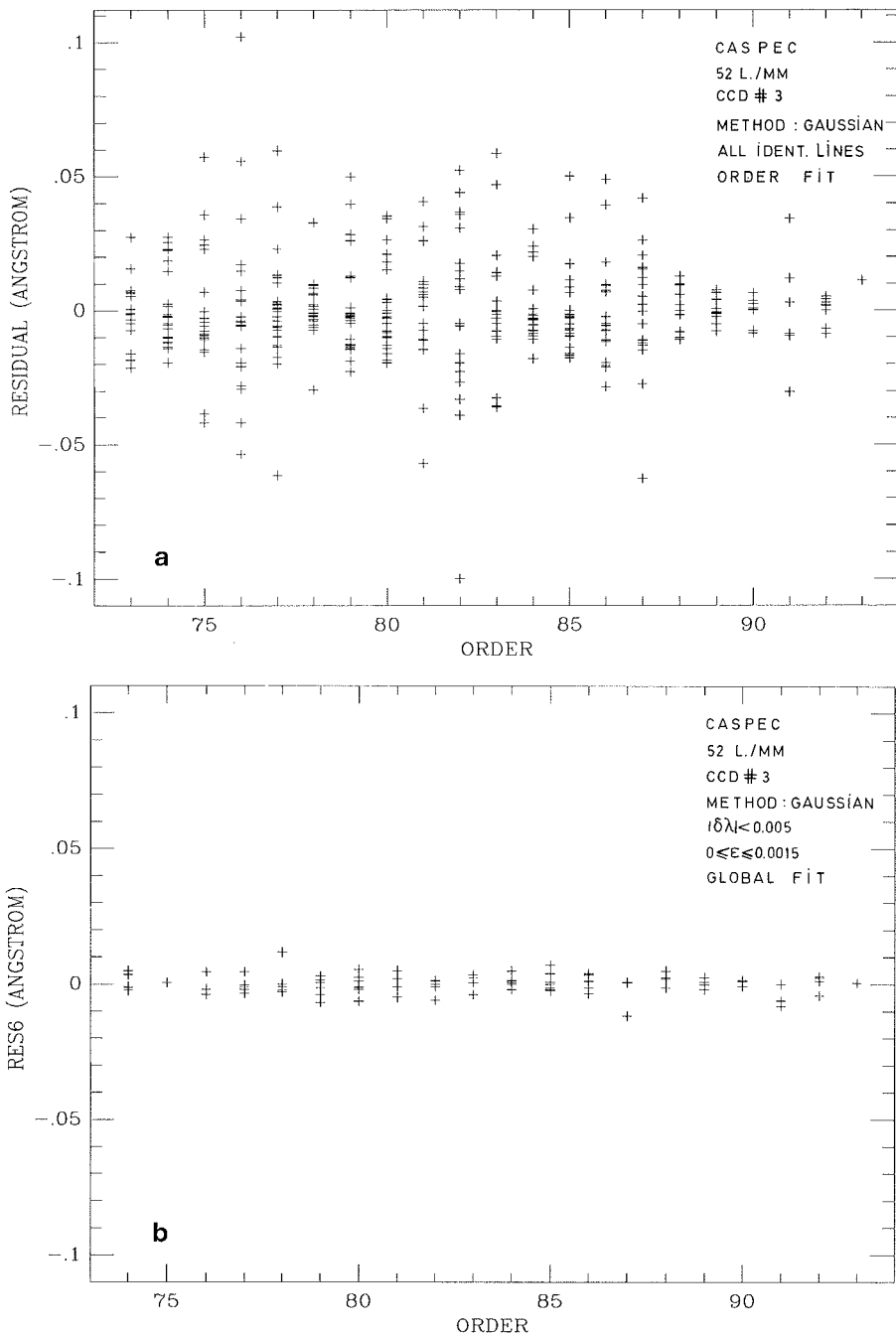
Figure 5: *Residuals in the wavelength calibration for the standard MIDAS procedure with gaussian fitting on all identified lines (5a) and in case of the proposed* global *fit using selected lines (5b).*

Table 1. *Approximate fit coefficients and the maximal contribution in absolute value of the corresponding terms. Last rows give r.m.s. of residuals with b_1 included as free parameter or fixed to 0.*

Coeff.	Frame 1 (Dec. 86)	Frame 2 (Jan. 88)	Max. contr. (Å)
a_0	3637.2	3635.6	constant
a_1	0.118	0.118	61.4
a_2	$-0.86\ 10^{-5}$	$-0.86\ 10^{-5}$	2.3
a_3	$-0.08\ 10^{-8}$	$-0.16\ 10^{-8}$	0.23
b_1	$-0.16\ 10^{-5}$	$-0.55\ 10^{-5}$	0.06
c_1	-0.010749	-0.010742	—
r.m.s.			
$b_1 = 0$	$4.6\ 10^{-3}$	$5.2\ 10^{-3}$	
b_1 = free	$4.5\ 10^{-3}$	$3.3\ 10^{-3}$	

blended lines relative to the global fit is only 0.3 km s^{-1}.

Figure 7 finally illustrates the adverse effect of the "gravity" method, showing the residuals to our global fit when this "gravity" method is used to define the actual line position. The residuals are plotted to the line centre-to-pixel centre position rather than to order number to show its (expected) dependence on that quantity.

Discussion and Conclusions

The effects of line blending and, to a lesser extent, the definition of line centre
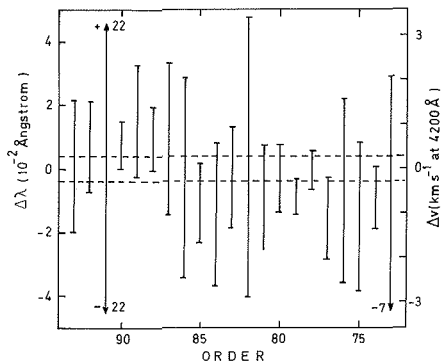
Figure 6: *Range of differences between the wavelength predicted by our global fit and that predicted by the standard MIDAS order-per-order fit. Labels indicating the larger ranges refer to the ordinate scale at the left ($\Delta\lambda$). The horizontal broken lines indicate +/− one standard deviation of the residuals in the global fit.*

by the "gravity" method, give dominant contributions to the residuals between predicted and measured line positions. They affect the wavelength calibration increasingly with the number of parameters allowed in the calibration fit. The global calibration fit $\lambda = \lambda$ (x, m*), deduced empirically from the regularities seen in provisionally made bivariate polynomial fits, has given excellent results i.e. residuals of about 0.03 pixel. Additional support for its validity comes from the fact that it predicted better than bivariate polynomials the wavelengths of the best (relatively weakly blended) not-selected lines, even when the polynomials were allowed to have up to 24 parameters.

Both the questions whether there is any theoretical support for this formula and whether it is (more) generally applicable to other echelles remain to be investigated. Since the mathematical form of λ (x, m*) should be obviously invariant for linear transformations in x and m* (i.e. for scaling and zero-point changes), the formula to be actually tested should contain at least an additional term in m* in the nominator,

$$\lambda (x, m^*) = \frac{(a_0 + b_0 m^*) + (a_1 + b_1 m^*) x + a_2 x^2 + a_3 x^3}{1 + c_1 m^*}$$

In our case b_0 appeared to be indistinguishable from 0, but it would not have been with any zero point definition.

Goodrich and Veilleux (1988) recently proposed a somewhat similar global formula, a bivariate polynomial in x and 1/m that might be conveniently written as

$$\Lambda (x, m) = \frac{1}{m} \sum_{k=0}^{2} (A_k + B_k m) x^k$$

They claim much higher residuals, 0.2 to 0.5 pixel. Since part of it might be due

to line blending effects (they start with about 600 calibration lines per frame and reject in up to 5 iterations outliers (residual >5 σ), but Figure 3 shows that such procedure is relatively inadequate (as statistically the probability that a blending line causes a given wavelength offset decreases smoothly with the size of the offset), we also tried to fit our selected data with this type of calibration formula. However, we did not obtain lower residuals, so that its usefulness is at best limited to the particular kind of echelle discussed by Goodrich and Veilleux (1988) for which it was intended. The main difference with our formula is the denominator, where we have m+constant instead of m, the constant being near to 1 in our case. It turns out that optimization of this constant is a necessary condition to obtain an accurate solution for CASPEC.

Our main conclusions are, that

(i) in order to achieve high precision in the wavelength calibration of CCD echelle spectra, a careful selection of reference lines is required, and the method "gaussian" should be used in the definition of line centre.

(ii) a global calibration model λ (x, m) describes accurately the measured line positions in the case of "blue" CCD CASPEC echelle spectra.

The success of the global model is essential with respect to (i) in so far that it permits to apply a stringent selection on the thorium-argon reference lines.

MIDAS users interested in an accurate wavelength calibration will find already part of the possibilities discussed here available in MIDAS. Presently, the portable MIDAS version already includes "gaussian" as default method. A catalogue of thorium-argon lines including indications on the blending of the lines in the wavelength range 3700–9000 Å is also available in Garching. This catalogue will be updated end 1989 to include our theoretical study of blending due to argon based on a wavelength list compiled by Norlén (1973). This reference contains accurate wavelengths for a large sample of the ArI and ArII lines seen in the CASPEC calibration spectra (it may also be useful to improve some argon wavelengths in the LINCAT tables) as well as for weaker lines that may nevertheless perturb thorium lines. The catalogue is an extension of the LINCAT tables in the sense that columns specifying our parameters $\delta\lambda$ and ε are added. The user might create his own selection from this catalogue by applying the SELECT/TAB command on the added columns and by adding the corrections $\delta\lambda$ to the (uncorrected) wavelengths in the first column. Although compiled for one specific dispersion, it remains useful at higher dispersion (e.g. smaller pixel size) when the selection is limited to almost unblended lines. It is believed that the definition of the risk factor through $\delta\lambda$ and ε leaves
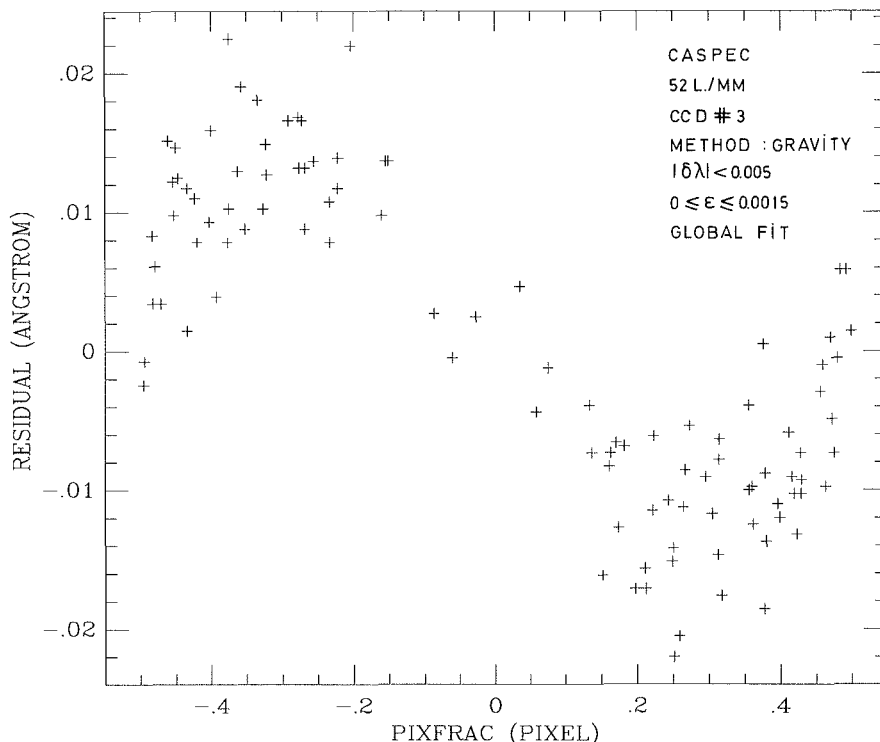
Figure 7: *Influence of the "gravity" method on the residuals in the wavelength calibration (global fit using selected lines). PIXFRAC is the "gravity" computed pixel fraction position of line centre.*

room for interpretation and generalization whenever necessary. Presently, ε includes uncertainties due to line centre-to-pixel centre position, window choice in the gaussian fitting (up to 7 pixels), FWHM of the PSF (up to 2 pixels). ε is provisionally set to a pre-defined code when there is *empirical* evidence for blending with argon lines. Blends with weaker argon lines undoubtedly remained unrecognized, especially above 4700 Å where the empirical test turned out to be less sensitive (among others due to the undersampling of the lines in the available frames).

At present, however, the user will have to specify his (own) global dispersion fit function using the possibility offered by MIDAS to define user functions, and he will himself have to take care of the transport of the coefficients in the system during the further reductions. Nevertheless, ESO is looking into the possibility to include the alternative of global dispersion formulae in future versions of the echelle package.

Acknowledgements

References

D'Odorico, S., Ponz, D.: 1984, *The Messenger* **37**, 24.
Goodrich, R.W., Veilleux, S.: 1988, *Publ. Astron. Soc. Pacific* **100**, 1572.
Norlén, G.: 1973, *Physica Scripta* **8**, 249.
Palmer, B.A., Engleman, R.Jr.: 1983, *Atlas of the Thorium Spectrum*, Los Alamos National Laboratory, ed. H. Sinoradzky.

Pushing CASPEC to the Limit

E.J. WAMPLER, ESO

Recent CASPEC users will have noticed that there is a continuing programme to upgrade the capabilities of the spectrograph. Together with electromechanical modifications of the spectrograph itself, there have been changes in the data reduction procedures. In addition, there is now substantially more experience with the biases that ESO reduction techniques introduce into the data. These improvements and the increased understanding of the critical processes can lead to a substantial increase in the limiting magnitude of CASPEC over that obtained in the past. Here I want to discuss some of the important choices to be made if good signal-to-noise (S/N) ratios, together with high resolution, is needed for faint objects. A general description of CASPEC has been given by D'Odorico et al. (1983).

The detector now used with CASPEC is RCA CCD number 8. This CCD has a readout noise equal to about 25 e^- when it is used with its controller operating at high gain. When observing faint objects, the CCD controller should be operated at the highest possible gain since faint sources do not tax the dynamic range of the system and a small step size in the analogue to digital conversion of the data reduces quantization errors when working at low signal levels.

CCD number 8 has several cosmetic and operational problems that affect its ability to detect weak signals. Between columns numbers 1 and 40 the background drops with increasing column number. Column numbers 40–45, 161 and 201 are always bright and must be discarded. For approximately 48 hours after the CCD has first been turned on, the dark current is high, initially as much as one hundred times the 2-3 e^- pix^{-1} hour^{-1} that is reached after a few days of operation. Therefore, observational programmes that are directed to the spectra of objects fainter than about mag 15 should be scheduled after programmes for brighter stars. CCD number 8 has some UV sensitivity but the sensitivity below about 4300 Å drops rapidly. It is possible to reach magnitude 14 or 15 at 3700 Å with a S/N ratio of about 50 after an integration time of several hours. At 5000 Å the gain in limiting magnitude over that at 3700 Å is about 2 magnitudes.

Even though the readout noise of CCD number 8 is lower than that of ESO's other RCA CCDs, this readout noise is still the dominating noise source when faint objects are observed. Therefore, the S/N ratio that can be achieved is directly proportional to the integration time rather than the square root of the integration time as is the case when the limiting noise source is not the detector noise. I have used integration times as long as 5 hours when observing faint sources. Such long integration times do result in a large number of cosmic ray events. However, the situation is not as bad as it may first appear; CCD number 8 is a high resolution CCD and the small, 15 μm square, pixel format greatly aids the identification and removal of cosmic ray events. Figure 1 shows the results of removing cosmic ray noise from CCD exposures on the 16.5-mag quasar UM402 = Q 020207-003. Figure 1a shows a three-hour frame before cleaning. In Figure 1b the lower threshold of the image was set to 280 DN, just above the highest level reached by the quasar signal. In Figure 1b nearly all the cosmic ray events are seen. Despite the large number of cosmic ray events seen in the figure, only about 1 % of all image pixels are affected by these cosmic rays. Filtering programmes, if used with a fixed threshold set to 280 DN (just above the highest level of the quasar signal), can be very effective in removing the cosmic ray tracks seen in this image. The cosmic ray impacts on the CCD generate a large number of electrons but these do not migrate very far in the Si substrate. The influence of a cosmic ray impact is confined to only a few pixels. Because these pixels are small, the contrast between the cosmic ray events and the photon signal from the spectrum is large. Leach (1988) has measured the cosmic ray e^- generation in CCDs. He finds that the differential pulse height distribution of cosmic ray generated electrons has a peak at about 400 e^-. This distribution is very skewed to high energy events; only a small fraction of all events produce fewer than 400 e^-.

The ESO RCA CCDs also show events caused by a local source of radioactivity. At least for CCD number 8, the local source has a pulse height distribution that is similar to that of the cosmic rays. An examination of the detected radiation events seen on long exposure frames taken with CCD number 8 indicates that aside from differences in the total counting rate, the cosmic ray model of Leach (1988) ade-